Valence band hybridization in N-rich $GaN_{1-x}As_x$ alloys

J. Wu,[1] W. Walukiewicz,[1,*] K. M. Yu,[1] J. D. Denlinger,[2] W. Shan,[1] J. W. Ager III,[1] A. Kimura,[3,†] H. F. Tang,[3] and T. F. Kuech[3]

[1]*Materials Sciences Division, Lawrence Berkeley National Laboratory, Berkeley, California 94720, USA*

[2]*Advance Light Source, Lawrence Berkeley National Laboratory, Berkeley, California 94720, USA*

[3]*Department of Chemical and Biological Engineering, University of Wisconsin-Madison, 1415 Engineering Drive, Madison, Wisconsin 53706-1691, USA*

(Received 5 May 2004; published 28 September 2004)

We have used photomodulated transmission and optical absorption spectroscopies to measure the composition dependence of interband optical transitions in N-rich $GaN_{1-x}As_x$ alloys with x up to 0.06. The direct band gap gradually decreases as x increases. In the dilute x limit, the observed band gap approaches 2.8 eV; this limiting value is attributed to a transition between the As localized level, which has been previously observed in As-doped GaN at 0.6 eV above the valence band maximum in As-doped GaN, and the conduction band minimum. The structure of the valence band of $GaN_{1-x}As_x$ is explained by the hybridization of the localized As states with the extended valence band states of GaN matrix. The hybridization is directly confirmed by soft x-ray emission experiments. To describe the electronic structure of the $GaN_{1-x}As_x$ alloys in the entire composition range a linear interpolation is used to combine the effects of valence band hybridization in N-rich alloys with conduction band anticrossing in As-rich alloys.

DOI: 10.1103/PhysRevB.70.115214 PACS number(s): 71.20.Nr, 78.20.−e, 74.70.Dd

I. INTRODUCTION

Recent progress in the materials synthesis methods has led to successful preparation of alloys composed of distinctly different semiconductor materials. The best known example of such highly mismatched alloys (HMAs) are dilute group III-N-V nitrides (i.e., $GaAs_{1-y}N_y$), in which the anions (i.e., As) in standard group III-V compounds are partially substituted with much more electronegative N atoms.[1] Incorporation of even small amounts of N produces large modifications of the electronic structure of the resultant alloys. The N-induced band gap reduction,[2,3] the enhanced electron effective mass[4] and the greatly reduced pressure dependence of the band gap[5] in these alloys deviate drastically from the linear interpolation between the end-point values that would be predicted by the virtual crystal approximation (VCA).

All the unusual properties of dilute group III-N-V HMAs have been explained by a band anticrossing (BAC) model.[1,3,5] In the BAC model, the anticrossing interaction between localized nitrogen states and the extended conduction band states of the host semiconductor modifies the electronic structure of the material. The BAC model has been successfully applied to other HMAs including dilute group II-O-VI alloys,[6,7] in which substitution of standard group VI anions with highly electronegative O leads to effects similar to those observed in the dilute nitrides.

Both the III-N-V and II-O-VI HMAs can be synthesized only in a very limited composition range. On the other hand, alloys such as $ZnSe_{1-x}Te_x$ or $ZnS_{1-x}Te_x$ show all the characteristics of HMAs,[8] including strong band gap bowing, and can be synthesized in the whole composition range. Our previous studies of these alloys have revealed different origins of the band-gap bowing for small ($x \rightarrow 0$) and large ($x \rightarrow 1$) Te contents.[9] On the Te-rich side, the reduction of the band gap is well explained by the BAC interaction between the Se or S localized states and the ZnTe conduction band states.[9] On the Se or S-rich side, the hybridization between the localized Te states and the valence bands of ZnSe or ZnS is responsible for the band-gap reduction and the rapid increase of the spin-orbit splitting.[9]

The As-rich $GaAs_{1-y}N_y$ and $GaInAs_{1-y}N_y$ alloys have been very widely studied and are now used in commercial optoelectronic devices.[1] In contrast, only a limited effort has been directed towards the synthesis of N-rich $GaN_{1-x}As_x$.[10–12] In most cases the As content was limited to impuritylike concentrations.[10,11] It was reported that the incorporation of impuritylike concentrations of As into GaN leads to a new emission band at about 2.6–2.7 eV.[11] The emission could be attributed to a localized, donorlike substitutional As_N state, which was theoretically predicted to have an energy level at about 0.4 eV above the valence band edge.[13]

In this paper we address the issue of the electronic structure of $GaN_{1-x}As_x$ alloys. We have used a variety of experimental techniques to study these N-rich alloys with up to 6.4 at. % of As. Our experimental results are well explained by the hybridization effects between localized As_N states and the extended valence band states. Combining the present results with the BAC model for the As-rich GaAsN alloys, we have developed a theoretical description of the electronic structure of these alloys that applies to the entire composition range.

II. EXPERIMENT

$GaN_{1-x}As_x$ layers with thickness of $\sim 0.15\ \mu$m were grown on 2 μm GaN templates on sapphire substrates by low pressure metal-organic vapor phase epitaxy. Growth details are described in previous publications.[12] Electron probe microanalysis (EPMA) and x-ray diffraction (XRD) were

used to determine the As content. The EPMA-determined As concentrations agree with the XRD measurements that assume a full layer relaxation; this indicates that the residual strain in the GaNAs layers is negligibly small.

The optical transition energies were measured using photomodulated transmission technique at room temperature. Quasimonochromatic light from a xenon arc lamp dispersed by a 0.5 m monochromator was focused on the sample as the probe beam. A chopped HeCd laser beam (325 nm) provided the modulation. The signals were detected by a Si photodiode using a phase-sensitive lock-in amplification system. Conventional optical absorption was measured on the same setup with the probe beam being chopped and the laser beam blocked. Nitrogen *K*-edge soft x-ray emission and absorption experiments were performed at Beamline 8.0 of the advanced light source in order to separately monitor the changes in the valence and conduction band partial density of states.

III. RESULTS AND DISCUSSION

A. RBS and PIXE results

The lattice location of the As atoms in GaNAs was studied by simultaneous rutherford backscattering spectrometry (RBS) and particle-induced x-ray emission (PIXE) experiments aligned in the $\langle 0001 \rangle$ axes using a 1.92 MeV $^4He^+$ beam. Backscattered He ions and characteristic x-rays excited by the He ions were detected by a Si surface barrier detector located at a backscattering angle of 165° and a Si(Li) detector located at 30°, respectively, with respect to the incident ion beam. The As content in the $GaN_{1-x}As_x$ films was also determined by PIXE. Figure 1 shows a comparison of the PIXE spectra of the $GaN_{1-x}As_x$ samples with $x=0$ and 0.0602. The As composition measured by the intensity of the As K_α signals is in agreement with that determined by x-ray diffraction.

Channeling RBS measurements in the $\langle 0001 \rangle$ axis directly indicate that the $GaN_{1-x}As_x$ films are of good crystalline quality with normalized yield χ (a ratio of the channeled yield to the corresponding random yield) ranging from 0.15 to 0.5. For a perfect crystal, χ is ~ 0.05. We observe that the crystalline quality degrades as x increases. The fraction of substitutional As atoms f_{sub} can be calculated by comparing the normalized yields of the GaN (RBS) and the As (PIXE) from the $GaN_{1-x}As_x$ films,

$$f_{sub} = \frac{1 - \chi_{As}}{1 - \chi_{GaN}}. \quad (1)$$

Figure 1(b) shows the substitutional As fraction measured by the channeling method as a function of the total As fraction. Except for the samples with high As content ($x > \sim 0.05$) the majority of the As ($\sim 80\%$) in the GaNAs films are substitutional.

B. Optical results

The upper portion of Fig. 2 shows typical absorption spectra obtained from the $GaN_{1-x}As_x$ alloys with x

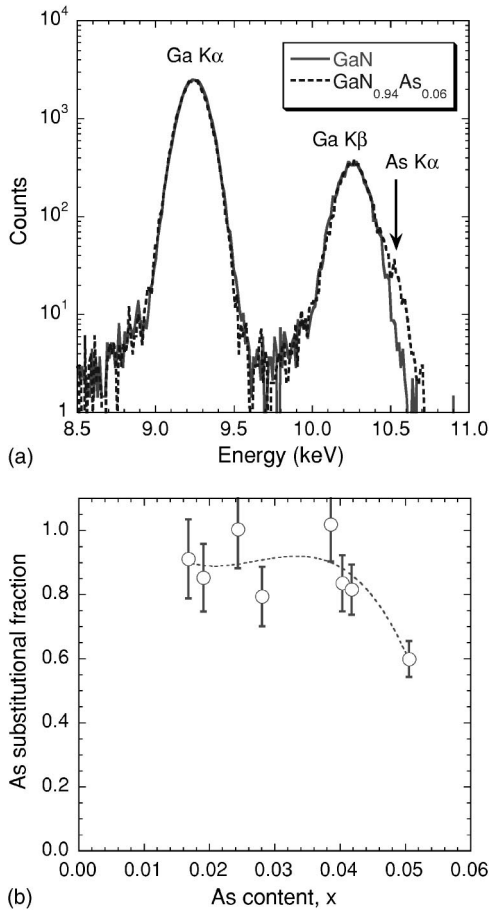

FIG. 1. (a) A comparison of the PIXE spectra of the GaNAs samples with $x=0$ and 0.06. (b) The substitutional As fraction measured by the channeling method as a function of the As composition.

$=0, 0.019$, and 0.060, respectively. The high-frequency oscillations on the curves are caused by the Fabry-Perot interference. It can be seen that as compared to GaN, the alloys show a more diffuse absorption edge toward the low-energy side. There would exist a large uncertainty if the gap energies are determined by the conventional method of extrapolating a part of the absorption coefficient squared down to the baseline. Therefore, photomodulated transmission (PT) measurements were carried out to better determine the transition energies associated with the bandgaps of the alloys.

Photomodulation spectroscopy is a differential method utilizing the modulation of the built-in electric field through photoinjected carriers by a periodically modulated light beam, such as the chopped laser beam used in this work. A change in the transmission ($\Delta T/T$) due to the modulation is proportional to the change of the imaginary part of the modulated dielectric function ($\triangle \varepsilon_2$).[14] The differential changes in the transmission appear as sharp derivativelike features in the modulated transmission spectrum, corresponding to specific critical transitions in the Brillouin zone. The results are shown in the lower portion of Fig. 2. The sharp features at ~ 3.4 eV correspond to the band-gap transitions in the GaN underlayers. The relatively broad features at lower energies are attributed to interband transitions across the band gap in the $GaN_{1-x}As_x$ layer.

It is interesting to note the behavior of the transitions in the alloy layer. The relative intensity of this feature increases as x increases, which suggests an increasing oscillator strength of the transition and an increasing density of states involved. It is also clear that the energy of this transition increases with decreasing x. Surprisingly, in the dilute limit ($x \to 0$) in $GaN_{1-x}As_x$, it converges to an energy position at $\sim$2.8 eV, as opposed to the band gap of GaN at 3.4 eV. This energy position is close to the well-known emission band (peaked at $\sim$2.7 eV) observed in As-doped GaN that has been attributed to As localized states.[11] We believe that the states involved in the PT transitions are derived from the As localized level. On the other hand, significant extended character must be incorporated into these states, as demonstrated by the strong oscillator strength of the transition in modulation spectroscopy. The situation is analogous to that of S(Se)-rich ZnSTe(ZnSeTe) alloys in which a new valence band is formed as a result of the hybridization of the Te localized states with the extended states of the ZnS(ZnSe) host.[9]

C. Hybridization between localized states and extended states

In As-rich $GaN_{1-x}As_x$ alloys ($x \to 1$), the BAC model predicts the formation of a new conduction sub-band from hybridization of the GaAs conduction-band states and the N localized level (E_N) that lies at 0.23 eV above the original conduction-band edge. The fundamental bandgap ($E_g^{As-rich}$) is the energy separation between the valence band edge and the bottom of this newly formed conduction band. The latter corresponds to the lower eigenenergy of the Hamiltonian formulated in degenerate perturbation theory,[3,5]

$$H_c^{As\text{-}rich} = \begin{bmatrix} E_c & C_{GaAs\text{-}N}\sqrt{1-x} \\ C_{GaAs\text{-}N}\sqrt{1-x} & E_N \end{bmatrix}, \qquad (2)$$

where E_c is the conduction band edge of GaAs, and $C_{GaAs\text{-}N}=2.7$ eV is the coupling parameter between E_c and E_N.[5] This conduction BAC model successfully explains the composition and hydrostatic pressure dependencies of the fundamental band gap on the As-rich side.[3,5]

In analogy to the anticrossing effect between the N localized level and the GaAs conduction band on the As-rich side, we calculate the hybridization between the localized As level and the valence bands of GaN for small As molar fractions. The original two Γ_9 and four Γ_7 valence bands as a function of x are described by the conventional 6×6 $\boldsymbol{k}\cdot\boldsymbol{p}$ matrix[15,16] with conduction and valence band energies set at corresponding VCA values. Influences from remote bands, including the lowest conduction band, are excluded in the interaction because of their large distance from the As localized level. An 8×8 Hamiltonian matrix is formed by augmenting the 6×6 matrix with two localized As states with energy E_{As} and opposite spins (i.e., $|E_{As}\uparrow\rangle$ and $|E_{As}\downarrow\rangle$). We choose the six momentum-decoupled wave functions as the basis for the valence band matrix. In this representation the matrix is written as

$$H_v^{N\text{-}rich} = \begin{array}{c} \begin{matrix} |11\uparrow\rangle & |11\downarrow\rangle & |10\uparrow\rangle & |10\downarrow\rangle & |1\bar{1}\uparrow\rangle & |1\bar{1}\downarrow\rangle & |E_{As}\uparrow\rangle & |E_{As}\downarrow\rangle \end{matrix} \\ \begin{bmatrix} F+\Delta & 0 & -H^* & 0 & K^* & 0 & -\frac{1-i}{\sqrt{2}}V & 0 \\ 0 & G+\Delta & \sqrt{2}\Delta_2 & -H^* & 0 & K^* & 0 & -\frac{1-i}{\sqrt{2}}V \\ -H & \sqrt{2}\Delta_2 & \lambda+\Delta & 0 & I^* & 0 & V & 0 \\ 0 & -H & 0 & \lambda+\Delta & \sqrt{2}\Delta_2 & I^* & 0 & V \\ K & 0 & I & \sqrt{2}\Delta_2 & G+\Delta & 0 & \frac{1+i}{\sqrt{2}}V & 0 \\ 0 & K & 0 & I & 0 & F+\Delta & 0 & \frac{1+i}{\sqrt{2}}V \\ -\frac{1+i}{\sqrt{2}}V & 0 & V & 0 & \frac{1-i}{\sqrt{2}}V & 0 & E_{As} & 0 \\ 0 & -\frac{1+i}{\sqrt{2}}V & 0 & V & 0 & \frac{1-i}{\sqrt{2}}V & 0 & E_{As} \end{bmatrix} \end{array}, \qquad (3)$$

where $|11\uparrow\rangle$ represents the direct product of the orbital wave function $|11\rangle=-(X+iY)/\sqrt{2}$ and the spin-up state $|\uparrow\rangle$, etc. In the Brillouin zone center ($\boldsymbol{k}=0$), the parameters in Eq. (3) are given by

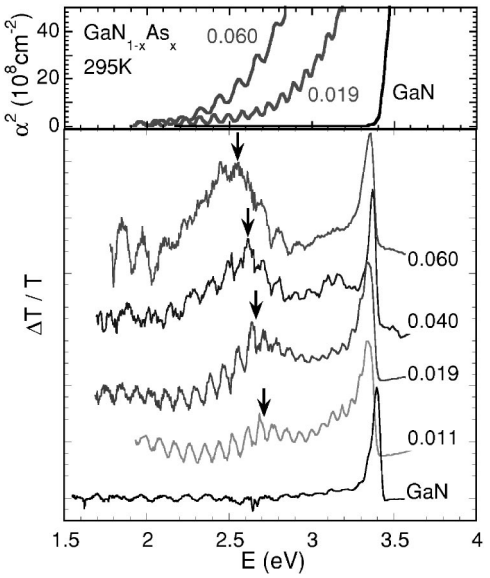

FIG. 2. Optical properties of N-rich GaNAs. Upper portion, the absorption coefficient squared of representative films. Lower portion, PT spectra of $GaN_{1-x}As_x$ with a range of compositions. The number beside each curve indicates the As fraction x. The arrows indicate the transition energies associated with the fundamental bandgap of the film.

$$\Delta = E_v(x) - [\Delta_1(x) + \Delta_2(x)], \tag{4a}$$

$$F = \Delta_1(x) + \Delta_2(x) + \lambda + \theta, \tag{4b}$$

$$G = \Delta_1(x) - \Delta_2(x) + \lambda + \theta, \tag{4c}$$

$$\lambda = D_1\varepsilon_{zz} + D_2(\varepsilon_{xx} + \varepsilon_{yy}), \tag{4d}$$

and

$$\theta = D_3\varepsilon_{zz} + D_4(\varepsilon_{xx} + \varepsilon_{yy}). \tag{4e}$$

In these equations, $E_v(x) = 2x$ is the VCA-predicted valence band edge of $GaN_{1-x}As_x$ with respect to that of GaN. $\Delta_1(x) = 0.0211(1-x)$ and $\Delta_2(x) = 0.0036(1-x) + 0.1133x$ are the crystal-field split and 1/3 of the spin-orbit split as predicted in the VCA frame, respectively.[15] ε_{xx}, ε_{yy}, and ε_{zz} are the strain tensors. H, I, and K are functions of the wave vector and are equal to zero at the Γ point.

In the matrix $H_v^{N\text{-}rich}$, V is the hybridization energy between the As localized states and the three basic crystal functions near the Brillouin zone center,

$$V \equiv \langle E_{As}|U|X\rangle = \langle E_{As}|U|Y\rangle = \langle E_{As}|U|Z\rangle = C_{GaN\text{-}As}\sqrt{x}. \tag{5}$$

In Eq. (5), we have assumed that crystal-field effects in the wurtzite lattice on the wave function of $|E_{As}\rangle$ are negligible, and that V has a square-root dependence on the impurity concentration similar to that obtained in the case of the conduction band hybridization.[3] $C_{GaN\text{-}As}$ is a parameter that describes the coupling strength and is to be determined by fitting with experimental data. The four doubly spin-degenerate eigenvalues of $H_v^{N\text{-}rich}$ have been computed by diagonalizing this 8×8 matrix. In the Brillouin zone center, they can be

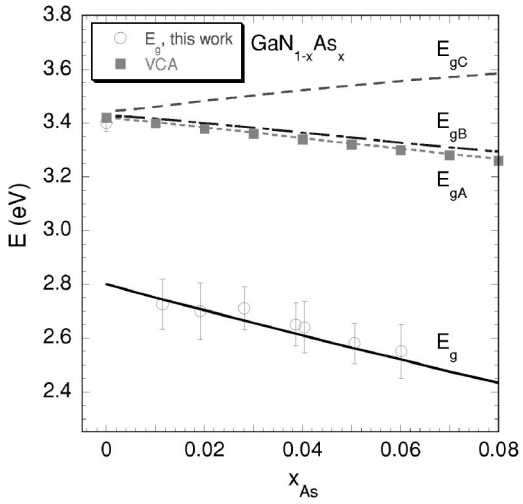

FIG. 3. E_g of $GaN_{1-x}As_x$ as a function of x measured by PT on the N-rich side. The curves show the calculated transition energies.

named, in the order of descending eigenenergy and according to the nature of their wave functions, as $E_{As\text{-}like}$, $E_{A\text{-}like}$, $E_{B\text{-}like}$, and $E_{C\text{-}like}$. Since the energy level of the As localized states is located above the top of the original valence band, a new edge of valence band is formed at the energy $E_{As\text{-}like}$. The fundamental bandgap in the N-rich $GaN_{1-x}As_x$, denoted as $E_g^{N\text{-}rich}(x)$, is attributed to the transition between the VCA conduction band edge and this newly formed valence band edge. The gap energies obtained from Fig. 2 are shown in Fig. 3 in comparison with the calculated results. The best agreement between the calculated $E_g^{N\text{-}rich}(x)$ and the experimental results is obtained by setting the coupling parameter $C_{GaN\text{-}As} = 0.75$ eV and $E_{As} = 0.62$ eV above the top of the valence band of GaN, as shown in Fig. 3. In the calculation we have assumed a flat alignment of the conduction band and a 2 eV offset of the valence band between GaAs and GaN.[16]

We note that due to the orthogonality between opposite spin states, some of the off-diagonal matrix elements in $H_v^{N\text{-}rich}$ between $|E_{As}\rangle$ and pure spin states are zero, such as $\langle 11\uparrow|E_{As}\downarrow\rangle$ and $\langle 11\downarrow|E_{As}\uparrow\rangle$. As a result, the Γ_9 heavy-hole band (band A) that consists of pure spin states does not mix with the As states at the Γ point; consequently the energy of the band A edge remains unchanged. The ban dgap E_{gA}, defined as the separation between the conduction band and the valence band A, thus follows the VCA gap energy that is a linear interpolation between GaN and GaAs, as can be seen in Fig. 3. The Γ_7 light hole (B) and especially the Γ_7 crystal-field (C) valence band edges, on the other hand, are pushed downwards by the anticrossing repulsion from the As level that lies at 0.62 eV above. The split between band A and band C is thus greatly enhanced from the original value (on the order of the crystal-field split $\sim$26 meV) to an order of magnitude larger (0.26 eV) at $x = 0.06$ .This anticrossing interaction not only shifts the band edge in the Brillouin zone center, but also affects the dispersion relations of the valence bands. By introducing wave-vector dependence into $H_v^{N\text{-}rich}$ through the parameters H, I, and K, the restructured dispersion relations, density of states and effective mass of the valence bands can be calculated. It is expected that the dis-

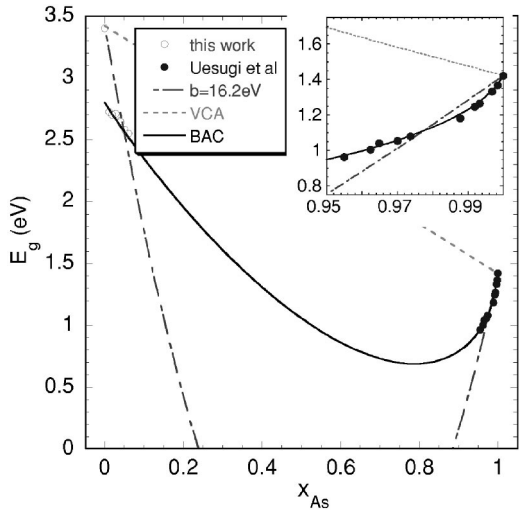

FIG. 4. E_g of $GaN_{1-x}As_x$ as a function of x over the entire composition range. The solid curve shows the band gap calculated from Eq. (6). The inset shows the region of the same plot near the As-rich end point.

persion relations become strongly nonparabolic, similar to the case in the conduction band anticrossing.[3]

As noted before, the GaNAs layers are nearly fully relaxed as confirmed by XRD experiments. The lattice mismatch between relaxed $GaN_{0.94}As_{0.06}$ and GaN is estimated to be about 1.5%. In the extreme case where the $GaN_{0.94}As_{0.06}$ layer is pseudomorphically strained on the GaN template, the strain-induced shift of the As-derived $E_g^{N\text{-}rich}$ was calculated to be less than 7 meV, and on E_{gA}, E_{gB}, and E_{gC} is ~23 meV, ~33 meV, and ~23 meV, respectively. The insensitivity of $E_g^{N\text{-}rich}$ to strain is due to the absence of the strain dependence (through λ and θ) in the As-states-related matrix elements in $H_v^{N\text{-}rich}$. Therefore, the strain effect, if exists at all, on the fundamental band gap of the $GaN_{1-x}As_x$ films studied in this work can be safely ignored.

D. Interpolation to the entire composition range

In order to fit the experimental data on both sides ($x \to 0$ and $x \to 1$) simultaneously and predict the band-gap bowing in the entire composition range ($0 \leqslant x \leqslant 1$), we adopt a linear interpolation scheme, similar in spirit to the original VCA interpolation, between these two effects, i.e., the conduction band BAC on the As-rich side[3,5] and the valence bands hybridization on the N-rich side. For the overall composition dependence of the fundamental bandgap, it is written as

$$E_g(x) = (1-x)\ E_g^{N\text{-}rich}(x) + x\ E_g^{As\text{-}rich}(x). \qquad (6)$$

This "linear" interpolation weights the importance of these two effects by the concentration of the majority component. Equation (6) well fits the fundamental band gap on both the As-rich[17] and the N-rich side of the $GaN_{1-x}As_x$ alloy system, as shown in Fig. 4. The calculated composition dependence of the bandgap reaches a minimum at $x \approx 0.8$ with a minimum band gap of 0.7 eV. Although $GaN_{1-x}As_x$ alloys with these high compositions are currently purely hypothetical, the excellent agreement of similar BAC calculations with experimental gap minimum in $ZnSe_{1-x}Te_x$ alloys ($E_g^{\min} \approx 2.1$ eV at $x \approx 0.7$)[9] leads us to believe that this predicted minimum gap in $GaN_{1-x}As_x$ is physically justifiable. This is in stark contrast to the composition dependence of the band gap predicted by a single-bowing-parameter fitting. As shown by the dotted-dashed line in Fig. 4, a forced quadratic fitting to the experimental gap energies on both sides yields a single bowing parameter of $b=16.2$ eV. This bowing parameter is in agreement with the value reported in Ref. 12. Along this quadratic curve, the bandgap would rapidly close up from both sides and become negative for $0.25 < x < 0.9$. In fact, it has been pointed out that the experimental bandgap on the As-rich side alone ($0.95 < x < 1$) cannot be fit with a single, constant bowing parameter,[18] as shown in the inset in Fig. 4. From our model this can be easily understood, as the eigensolutions of the matrices in Eqs. (2) and (3) are not simple quadratic functions of composition.

We also note that in our calculation we have used the band parameters of wurtzite GaN and zinc-blende GaAs. The GaNAs alloys grown on the N-rich side are wurtzite and on the As-rich side are zinc-blende structured. Therefore, a structural phase transition would occur at some composition if the GaNAs alloys could be grown over the entire composition range. A simpler theoretical picture might be to consider the alloys formed between isostructural GaN and GaAs. However, the main differences of zinc-blende GaN from wurtzite GaN at the Γ point are only the band-gap reduction ($\triangle E_g \approx 0.2$ eV) and the absence of the crystal-field split (0.021 eV), both being small on the scale of the $GaN_{1-x}As_x$ band gap. We thus do not expect drastic difference of the picture for purely zinc-blende $GaN_{1-x}As_x$ alloys.

In our theoretical description of the composition dependence of the energy, we consider separately the shifts of the conduction and the valence band edges relative to the localized levels of nitrogen and arsenic, respectively. This allows the prediction of the composition dependence of the locations of the conduction minimum and the valence band maximum relative to a common energy reference. As is shown in Fig. 5, the conduction band edge exhibits a broad, deep minimum at $x \approx 0.62$, whereas the valence band maximum energy increases monotonously with increasing As content.

The doping behavior of the GaNAs alloys can be better understood in the context of our model of the electronic structure across the entire composition range. The efficiency of doping a semiconductor n or p type depends on the relative position of its conduction and valence band edges with respect to a universal amphoteric defect level named Fermi stabilization level (E_{FS}, see Fig. 5).[20,21] Semiconductors with conduction (valence) band edge close to E_{FS} can be easily doped $n(p)$ type but not $p(n)$ type. E_{FS} is located at ~4.9 eVbelow the vacuum level, and is near the middle of the bandgap of GaAs but far from the valence band edge of GaN.[21] This explains the notorious inefficiency of p type doping in GaN. As has been shown previously, the N-induced downward shift of the conduction band edge of GaAs greatly improves the activation efficiency of shallow donors in As-rich GaNAs alloys.[22] The maximum achievable free-electron concentration in GaAs can be increased by

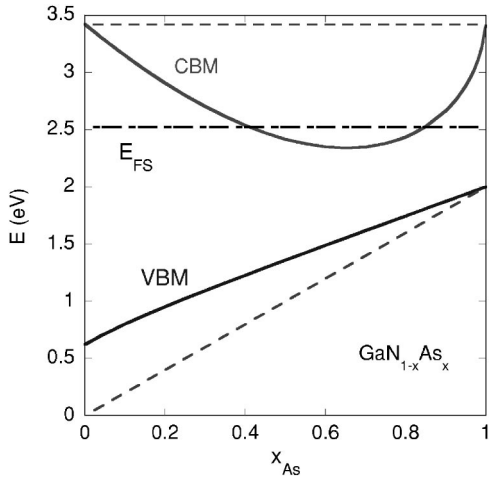

FIG. 5. Predicted composition dependence of the conduction band minimum (CBM) and the valence band maximum (VBM) energy. The linear interpolations of CBM and VBM between end point compounds (GaN and GaAs) are shown by dashed lines. E_{FS} represents the Fermi level stabilization energy.

more than 20 times by incorporating 3.3% N into GaAs. In the view of the discovery of the valence band hybridization in N-rich GaNAs, we expect that the As-induced upward shift of the valence band edge should also improve the activation efficiency of acceptors in the host GaN.

E. Soft x-ray fluorescence experiments

The hybridization model predicts an upward shift of the valence band edge in N-rich $GaN_{1-x}As_x$ that causes the abrupt reduction in the band gap. For a direct test of this model one needs to measure the relative positions of the top of the valence band in these alloys. We have used the combination of soft x-ray emission (SXE) and absorption (XAS) spectroscopies to investigate the partial density of states of the conduction band and valence band as a function of composition.[19] XAS was detected by the total electron yield (TEY) with an energy resolution of 0.1 eV, and SXE was measured using the Tennessee/Tulane grating spectrometer with a total energy resolution of 0.6 eV. XAS energies were calibrated to N_2 gas phase absorption and SXE energies were aligned to XAS using elastic emission as a marker for the excitation energy.

Figure 6 shows the SXE and XAS spectra for a number of $GaN_{1-x}As_x$ samples excited at the nitrogen *K*-edge. The energy of the excitation x-ray first scanned across the N *K*-edge, and the TEY was recorded as the XAS. The threshold energy of the excitation defines the conduction band minimum with respect to the *K*-edge. They are shown as the right-hand part of the curves in Fig. 6. The excitation energy was then tuned to the onset of the conduction band ($\sim$398 eV) and the resultant SXE due to electronic transitions from the upper valence band to the N *K*-shell was recorded with a wavelength-dispersive detector. The SXE spectrum is shown in Fig. 6 on the left-hand side. In this way the absolute positions of the conduction band and valence band edges are directly measured as a function of composition and compared to the results of conventional optical measurements. The first global observation in Fig. 6(a) is the change in amplitude and line-shape of the SXE and XAS spectra. In these spectra the raw experimental relative intensities have been preserved; i.e., within the SXE or the XAS set, the intensities shown are directly proportional to their raw experimental data and the proportional coefficient is the same for all samples. The XAS changes of the overall peak broadening and suppression of the 408 and 410 eV peaks can be attributed to the decreasing crystallinity for increasing As concentration, consistent with RBS observations. Similarly, the increased SXE intensity combined with a shift to lower energy can be attributed to the loss of direct-gap ***k***-selectivity at threshold excitation, also resulting from a decrease in crystallinity and/or the introduction of localized As states.

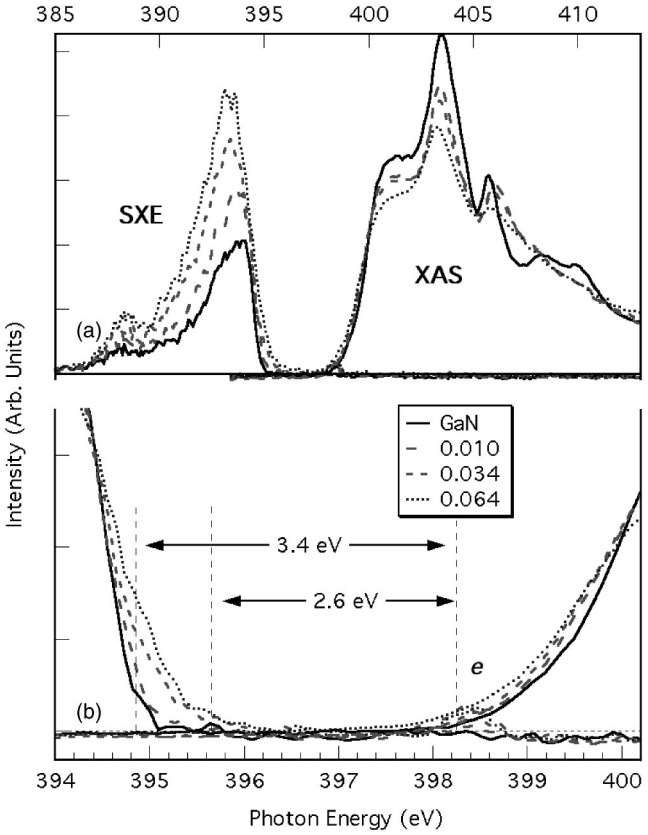

FIG. 6. Nitrogen *K*-edge SXE and XAS of $GaN_{1-x}As_x$ films with different As fractions. The numbers in the legend indicate the As fraction *x*. An elastic emission peak (*e*) in the threshold-excited SXE is used for energy calibration to XAS.

More important for this study is the relative changes in the threshold energies of the SXE and XAS, shown in details in Fig. 6(b). Consistent with the model predictions illustrated in Fig. 5, the XAS conduction band minimum shows a small ($<$0.25 eV) downwards shift with increasing As content, while the SXE valence band edge shows a more distinct development of additional density of states and larger upwards energy shift of $\sim$0.8 eV. The top of the valence band of GaN is mostly derived from the N *p*-states, so that the dipole transitions to the *K*-shell of N atoms result in strong x-ray emission reflective of the N-*p* partial density of states. The extra density of states that emerges on the SXE spectra

corresponds to the $E_{As\text{-}like}$ states that is derived from the As localized states but hybridized with the valence band states of GaN(N *p*-states). The less abrupt shift of the valence band edge in Fig. 6, as compared to the one determined by the modulation spectroscopy shown in Fig. 3, is a consequence of the much more element selectivity in the detection of the N-*p* partial density states in the SXE technique. For example, the admixture of N *p*-states in the $|E_{As\text{-}like}\rangle$ valence band edge was calculated to be only $\sim 5\%$ at $x=0.01$. The SXE thus does not resolve the shift until a significant amount of N *p*-states is admixed into the $|E_{As-like}\rangle$ valence-band edge.

IV. CONCLUSIONS

In summary, we have demonstrated that the valence band of N-rich $GaN_{1-x}As_x$ alloys converges to the donorlike As localized energy level that was previously observed in As-doped GaN. The composition dependence of the fundamental band gap is explained by considering the hybridization between the As localized states and the valence-band states of GaN. A linear interpolation between the valence band hybridization on the N-rich side and the conduction band anticrossing on the As-rich side accounts for experimental data on both sides. The band gap of the $GaN_{1-x}As_x$ system is predicted to reach a minimum at 0.7 eV for a composition of $x \approx 0.8$.

ACKNOWLEDGMENTS

This work (including the part done at the Advance Light Source) was supported by the Director, Office of Science, Office of Basic Energy Sciences, Division of Materials Sciences and Engineering, of the U.S. Department of Energy under Contract No. DE-AC03-76SF00098.

*Electronic address: w_walukiewicz@lbl.gov
†On leave from Photonic and Wireless Devices Research Laboratories, NEC Corporation, Otsu-shi, Shiga 520-0833, Japan.

[1] See, for example, special issue on III-N-V semiconductor alloys, Semicond. Sci. Technol. **17**(8), 741–906 (2002).
[2] M. Weyers, M. Sato, and H. Ando, Jpn. J. Appl. Phys., Part 1 **31**, L853 (1992).
[3] J. Wu, W. Shan, and W. Walukiewicz, Semicond. Sci. Technol. **17**, 860 (2002).
[4] C. Skierbiszewski, P. Perlin, E. Wisniewski, W. Knap, T. Suski, W. Walukiewicz, W. Shan, K. M. Yu, J. W. Ager III, E. E. Haller, J. F. Geisz, and J. M. Olson, Appl. Phys. Lett. **76**, 2409 (2000).
[5] W. Shan, W. Walukiewicz, J. W. Ager III, E. E. Haller, J. F. Geisz, D. J. Friedman, J. M. Olson, and S. R. Kurtz, Phys. Rev. Lett. **82**, 1221 (1999).
[6] J. K. M. Yu, W. Walukiewicz, J. Wu, J. W. Beeman, J. W. Ager, E. E. Haller, I. Miotkowski, A. K. Ramdas, and P. Becla, Appl. Phys. Lett. **80**, 1571 (2002).
[7] K. M. Yu, W. Walukiewicz, J. Wu, W. Shan, J. W. Beeman, M. A. Scarpulla, O. D. Dubon, and P. Becla, Phys. Rev. Lett. **91**, 246403 (2003).
[8] W. Walukiewicz, W. Shan, K. M. Yu, J. W. Ager, III, E. E. Haller, I. Miotkowski, M. J. Seong, H. Alawadhi, and A. K. Ramdas, Phys. Rev. Lett. **85**, 1552 (2000).
[9] J. Wu, K. M. Yu, W. Walukiewicz, J. W. Ager, III, E. E. Haller, I. Miotkowski, A. K. Ramdas, C.-H. Su, I. K. Sou, R. C. C. Perera, and J. D. Denlinger, Phys. Rev. B **67**, 035207 (2003).
[10] K. Iwata, H. Asahi, K. Asami, R. Kuroiwa, and S. Gonda, Jpn. J. Appl. Phys., Part 1 **37**, 1436 (1998).
[11] S. V. Novikov, A. J. Winser, A. Bell, I. Harrison, T. Li, R. P. Campion, C. R. Staddon, C. S. Davis, F. A. Ponce, and C. T. Foxon, J. Cryst. Growth **240**, 423 (2002).
[12] A. Kimura, C. A. Paulson, H. F. Tang, and T. F. Kuech, Appl. Phys. Lett. **84**, 1489 (2004); A. Kimura, H. F. Tang, and T. F. Kuech, J. Cryst. Growth **265**, 71 (2004).
[13] T. Mattila and A. Zunger, Phys. Rev. B **58**, 1367 (1998).
[14] D. E. Aspnes, in *Optical Properties of Solids*, edited by M. Balkanski (North-Holland, Amsterdam, 1980), Chap. 4A.
[15] G. B. Ren, Y. M. Liu, and P. Blood, Appl. Phys. Lett. **74**, 1117 (1999); Yu. M. Sirenko, J. B. Jeon, K. W. Kim, M. A. Littlejohn, and M. A. Stroscio, Phys. Rev. B **53**, 1997 (1996).
[16] S. Tiwari and D. J. Frank, Appl. Phys. Lett. **60**, 630 (1992); G. Martin, A. Botchkarev, A. Rockett, and H. Morkoc, *ibid.* **68**, 2541 (1996).
[17] K. Uesugi, N. Marooka, and I. Suemune, Appl. Phys. Lett. **74**, 1254 (1999).
[18] U. Tisch, E. Finkman, and J. Salzman, Appl. Phys. Lett. **81**, 463 (2002).
[19] L. C. Duda, C. B. Stagarescu, J. Downes, K. E. Smith, D. Korakakis, T. D. Moustakas, J. H. Guo, and J. Nordgren, Phys. Rev. B **58**, 1928 (1998).
[20] W. Walukiewicz, Appl. Phys. Lett. **54**, 2094 (1989); D. D. Nolte, Solid-State Electron. **33**, 295 (1990).
[21] W. Walukiewicz, Physica B **302**, 123 (2001).
[22] K. M. Yu, W. Walukiewicz, W. Shan, J. W. Ager III, J. Wu, E. E. Haller, J. F. Geisz, D. J. Friedman, and J. M. Olson, Phys. Rev. B **61**, R13 337 (2000).